Biochemistry

pubs.acs.org/biochemistry Article

Protein Dynamics Influence the Enzymatic Activity of Phospholipase A/Acyltransferases 3 and 4

Soumya Deep Chatterjee, Juan Zhou, Rubin Dasgupta, Anneloes Cramer-Blok, Monika Timmer, Mario van der Stelt, and Marcellus Ubbink*

Cite This: *Biochemistry* 2021, 60, 1178–1190 Read Online

ACCESS | Metrics & More | Article Recommendations | Supporting Information

ABSTRACT: Phospholipase A/acyltransferase 3 (PLAAT3) and PLAAT4 are enzymes involved in the synthesis of bioactive lipids. Despite sequential and structural similarities, the two enzymes differ in activity and specificity. The relation between the activity and dynamics of the N-terminal domains of PLAAT3 and PLAAT4 was studied. PLAAT3 has a much higher melting temperature and exhibits less nanosecond and millisecond dynamics in the active site, in particular in loop L2(B6), as shown by NMR spectroscopy and molecular dynamics calculations. Swapping the L2(B6) loops between the two PLAAT enzymes results in strongly increased phospholipase activity in PLAAT3 but no reduction in PLAAT4 activity, indicating that this loop contributes to the low activity of PLAAT3. The results show that, despite structural similarity, protein dynamics differ substantially between the PLAAT variants, which can help to explain the activity and specificity differences.

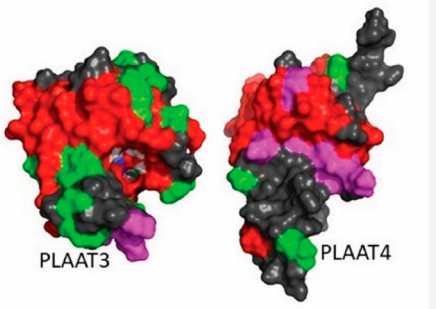

INTRODUCTION

Phospholipase A/acyltransferases (PLAATs) are a five-membered family of enzymes. They were first identified as H-Ras-like class II tumor suppressors (HRASLS).[1] Numerous studies in different scientific domains led to a variety of names (Table S1). The five members are part of a larger, diverse superfamily of NlpC/P60 thiol proteases or papain-like proteases because of their sequence similarity with lecithin: retinol acyltransferases (LRAT), a member of the NlpC/P60 family.[2] PLAATs share a highly conserved sequence NCEHFV, which contains the catalytic cysteine that acts as the nucleophile.[2−5] The cysteine is part of a catalytic triad that also contains two histidine residues, one acting as the base that deprotonates the sulfhydryl group of the nucleophile and the other stabilizing the imidazole ring of the basic histidine in PLAAT2−5. In PLAAT1, the second histidine is replaced by asparagine. This CHH catalytic triad is a hallmark signature of the NlpC/P60 superfamily of proteins.[2,6−8] Four of the PLAAT enzymes are membrane anchored proteins having a C-terminal trans-membrane domain, while PLAAT5, the largest of all PLAATs, lacks this anchor.[9] The structures of PLAAT2, PLAAT3, and PLAAT4 have been reported (Figure 1).[2,7,8] Depending on the structure, the secondary structure comprises three or four α-helices and an antiparallel β-sheet containing five or six strands, similar to classic segregated $\alpha+\beta$-folds of papain-like proteases.[2,6] The PLAATs catalyze the formation of *N*-acyl phosphatidyl ethanolamines (NAPE), which undergo further conversions to form *N*-acylethanolamines (NAEs), an important class of bioactive lipids that plays a variety of roles in processes such as anti-inflammation (*N*-palmitoyethanolamine)[10−12] and catabolism of fat (*N*-oleoylethanolamine),[13] and they have antiapoptotic activity (*N*-stearoylethanolamine)[13] and act as ligands for cannabinoid receptors (*N*-arachidonoylethanolamine, anandamide).[14−16]

PLAATs, as the name indicates, demonstrate phospholipase $A_{1/2}$ ($PLA_{1/2}$) activities with both phosphatidylcholine (PC) and phosphatidylethanolamine (PE) acting as substrates.[3,9,17−20] All PLAATs except PLAAT3 show specificity for the *sn*-1 position, whereas it has been suggested that PLAAT3 may prefer either the *sn*-1 or the *sn*-2 position, depending on the type of substrate and assay conditions.[21−23] The second part of the name comes from the ability to transfer the acyl-chain of a phosphoglyceride, for example PC, to the amino group of PE, leading to the formation of NAPEs. Furthermore, PLAATs can act as O-acyltransferases, transferring an acyl-chain to the *sn*-1 or *sn*-2 position of a lysophospholipid, for example lysophosphatidylcholine.[2,3,17,19,24] PLAAT3 is found mostly in white adipose tissue and less in brown adipose tissue.[21,25] In white adipose tissue, it modulates lipolysis and therefore is a critical factor in obesity, as was elegantly demonstrated in mice models by Jaworski et al.[25] PLAAT3 was discovered as being a tumor suppressor;[20,26−32] however, other reports showed that PLAAT3

Received: December 20, 2020
Revised: March 4, 2021
Published: March 22, 2021

https://doi.org/10.1021/acs.biochem.0c00974
Biochemistry 2021, 60, 1178−1190

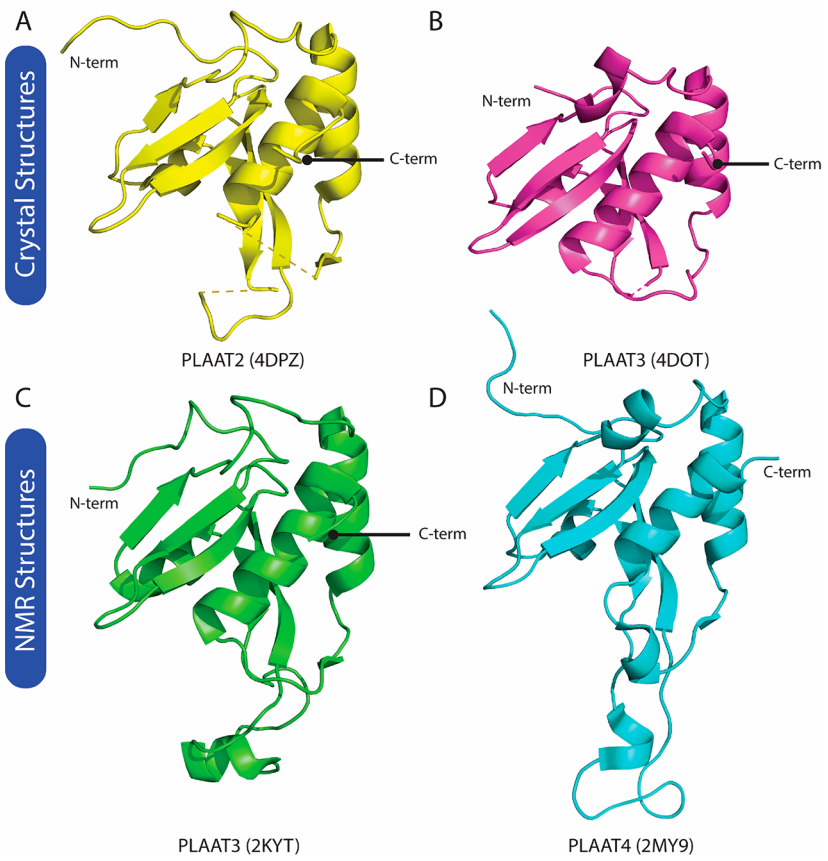

Figure 1. Crystal (A and B) and NMR (C and D) structures of PLAAT2, PLAAT3, and PLAAT4. The PDB entry codes are indicated in brackets.[2,7,8] Dashed lines in A and B are indicated for visual continuity of the loops.

increases tumor progression.[29,33] PLAAT3 shows a preference for PLA activity over *N*-acyltransferase activity.[17,24] PLAAT4 is found in keratinocytes, where it activates transglutaminase I (TG1), which in turn produces a cornified envelope, necessary for cell proliferation and survival, and skin to function as a physical and water barrier.[34−37] PLAAT4 was shown to work as a class II tumor suppressor and is downregulated in psoriasis and skin cancer.[38−44] PLAAT4 is a homologue of PLAAT3, showing 58% sequential identity and 72% similarity,[38,39] and it also shows more $PLA_{1/2}$ activity than *N*-acyltransferase activity.[17,19,24] However, the two enzymes exhibit a contrasting characteristic regarding the $PLA_{1/2}$ activity. The transmembrane C-terminal domain (CTD) is crucial for PLAAT3 $PLA_{1/2}$ activity, and truncation of this domain has been shown to result in loss of phospholipase activity by Uyama et al.[45] In contrast, Golczak et al.[2] demonstrated that, unlike truncated PLAAT3, truncated PLAAT4 is capable of phospholipase activity, suggesting that the transmembrane C-terminal domain is not critical for PLAAT4 $PLA_{1/2}$ activity. Furthermore, these authors demonstrated that the truncated PLAAT4 is the more active phospholipase. Clearly, despite the structural similarities, the activity depends both on the exact sequence and the truncation. We wondered whether differences in protein dynamics could explain the differences in activity. In the current study, the dynamics of the soluble N-terminal domains (NTDs) of PLAAT3 and PLAAT4 were probed using NMR spectroscopy on the nanosecond and millisecond time scales. The results show that generally PLAAT4 is more flexible on the nanosecond time scale and exhibits more millisecond dynamics around the active site than PLAAT3. MD calculations support these findings and suggest that one particular active site loop could influence activity. A loop-swapping mutagenesis experiment shows that PLAAT3 gains activity with the loop taken from PLAAT4. The reasons for the differences in dynamics and the relevance of these findings for the full-length proteins are discussed.

MATERIALS AND METHODS

Construction of DNA Fragments. DNA sequences encoding the human N-terminal soluble form (residues 1−125) of PLAAT3 or PLAAT4 (Uniprot ID P53816 and Q9UL19, respectively) with N-terminal His_6 tag and a TEV cleavage site were ordered from GeneArt. The fragments were inserted in-frame into the bacterial expression vector pET-28a using the *Nco*I and *Xho*I restriction sites. Fragment-based mutagenesis[46] was carried out by forward and reverse primers designed to swap the L2(B6) loop of PLAAT3 (103E-V-L-Y-K-L-T-S-E111) with that of PLAAT4 (103K-M-K-Y-S-I-V-S-R111) and vice versa.

Protein Production and Purification. Chemically competent *Escherichia coli* BL21-DE3pLys cells were transformed with the plasmids for protein production. The bacteria were cultured overnight in 50 mL of LB medium with 50 μg/mL kanamycin at 37 °C under shaking. For ^{15}N-labeling, 5 mL of the overnight preculture was transferred to 500 mL minimal medium with 50 μg/mL kanamycin. When the OD_{600} reached 0.6, the temperature was lowered to 22 °C, and gene expression was induced by addition of 0.5 mM IPTG. The culture was incubated for 5 h before cells were harvested by centrifugation at 6000 rpm at 4 °C. The pellet was

https://doi.org/10.1021/acs.biochem.0c00974
Biochemistry 2021, 60, 1178−1190

resuspended in 5 mL of 50 mM Tris−HCl buffer (pH 7.5) followed by freezing at −80 °C overnight. The cells were thawed the next day in the presence of DNase I and lysozyme and lysed using a French press. The lysate was centrifuged at 4 °C at 25 000*g* for 45 min. The supernatant of the cell lysate containing the His_6-tagged soluble protein was then loaded on a HiTrap-Nickel column equilibrated with 50 mM Tris pH 7.5, 500 mM NaCl, and 5 mM imidazole. The protein was eluted using a linear imidazole concentration gradient from 0 to 0.5 M. The collected fractions were pooled and dialyzed overnight using a 3.5 kDa molecular weight cutoff cellulose membrane at 4 °C in 50 mM Tris, pH 7.5, 500 mM NaCl, 0.5 mM EDTA buffer to remove imidazole. His_6-tagged TEV protease was added for the cleavage of the His_6-tag on PLAAT during dialysis overnight. The mixture was loaded again on a His_6-Trap Nickel column to collect the N-terminal PLAAT3 and PLAAT4 domains. The buffer was changed into 50 mM Tris-HCl, 50 mM NaCl, 10 mM DTT, pH 7.5. The volume of the sample was reduced to 2.5 mL using a 5 kDa MWCO Amicon Ultracentrifugal filter (EMD Millipore) at 2200*g* and 15 °C. The concentrated sample was loaded on and eluted from a Superose12 gel filtration column in 30 mM sodium phosphate buffer with 30 mM NaCl and 10 mM DTT at pH 7.0. All NMR samples contained 1.5 mM uniformly ^{15}N -labeled protein in this buffer with 7% D_2O added for lock.

Thermofluor-Based Melting Temperature (T_m) Analysis. Thermofluor analysis was performed on a CFX96 Real-Time PCR system (Bio-Rad) to determine the thermal stability of PLAAT proteins. Duplicate protein samples of 25 μL were prepared in 30 mM sodium phosphate buffer (pH 7.0), 25 mM sodium chloride, and 10 mM DTT in 96-well Concord Polycarbonate PCR plates (Bio-Rad) using SYPRO Orange (Sigma-Aldrich) as a fluorescent probe. After sealing with Optical-Quality Sealing Tape (Bio-Rad), plates were vortexed and centrifuged for 30 s using an MPS 1000 mini PCR Plate Spinner (Labnet). Melting curves were obtained by detection of fluorescence using the FRET channel of the RT-PCR machine. The temperature was increased in steps of 0.5 °C increments. At each point, the sample was incubated for 30 s before measuring the fluorescence. At the end, the reaction was stopped by heating at 90 °C for 5 min. The results were analyzed in CFX Manager 3.1 (Bio-Rad). The temperature corresponding to the maximum of the first derivative of the melting curve was taken to be the melting temperature (T_m).

Phospholipase Assay. Protein solutions (200 μL, 0.1 mg/mL) were diluted with equal volumes of buffer A (50 mM Tris-HCl, pH 8, 50 mM NaCl, 2 mM DTT). These solutions were added to white 96-well plates (60 μL per well, in triplicate). A standard dilution series of the product BODIPY FL-Cs (ThermoFischer Scientific) was prepared in pure DMSO in the following concentrations: 0.0 μM (pure DMSO), 0.005, 0.01, 0.05, 0.1, 0.5, and 1 μM. The product was diluted with a 1:1 mixture of buffer A and buffer B (50 mM Tris-HCl pH 8, 100 mM NaCl, 1 mM $CaCl_2$). The solutions of standards were added in the 96-well plate (100 μL each). The liposome mixture was prepared by mixing DOPC (5.1 μL, 10 mM stock in ethanol), DOPG (5.1 μL, 10 mM stock in ethanol), and the substrate Red/Green BODIPY PC-A2 dissolved in pure DMSO (5.1 μL, 1.5 mM, ThermoFischer Scientific). The mixture was injected slowly (in about 45 s) under vortexing into a glass vial containing 1.5 mL of assay buffer using a pipet fitted with a narrow orifice gel-loading tip. The liposome mixture (50 μL) was added to each well of the 96-well plate in which the enzymes were to be tested. Then, PLAAT protein solutions (50 μL) were transferred from the white 96-well plate to the black microplate wells containing the liposome mixture at 37 °C. The fluorescence measurement was started immediately, every 20 s in 60 min on a Tecan GENios with a gain of about 54 and an excitation filter at 488 nm and emission filter at 530/590 nm.

T_1, T_2, and NOE Measurements. NMR experiments were carried out at 25 °C on 600 and 850 MHz Bruker Avance III spectrometers equipped with TCI cryoprobes. Standard Bruker pulse sequences were used for T_1 (hsqct1etf3gpsitc3d), T_2 (hsqct2etf3gpsitc3d), and NOE (hsqcnoef3gpsi) experiments. $^{15}N-^{1}H$ NOE spectra with and without amide proton saturation were recorded in an interleaved fashion recording 80 transients per point, yielding very high signal-to-noise data. The final HSQC spectra contained 2048 and 200 points in the ^{1}H and ^{15}N dimensions, respectively. In the T_1 and T_2 experiments, water saturation was avoided using low power water-flip-back pulses. The mixing times (s) used for the determination of T_1 were 0.01 (2×), 0.16, 0.22, 0.35 (2×), 0.48, 0.6, 0.8 (2×), 1.0, and 1.2 with duplicates for error estimation. Mixing times (s) for T_2 determination were 0, 0.034 (2×), 0.05, 0.07 (2×), 0.085, 0.10, 0.135 (2×), 0.17, 0.2 (2×), and 0.24. A recycle delay of 4 s was used for all T_1, T_2, and NOE experiments. All spectra were processed with Bruker TOPSPIN with linear prediction applied to the ^{15}N dimension and qsine and Gaussian window functions. NOE values were calculated as the ratio of peak intensities in the experiment with and without proton saturation. To obtain T_1 and T_2 values, the experimental data points (peak heights) were fitted to a curve $I_0 \times \exp(-t/T_i)$, where I_0 is the peak intensity of the reference spectra, and fit parameter errors were estimated using Monte Carlo simulations. All NOE, T_1, and T_2 analyses were performed using the Bruker Protein Dynamics software suite. $^{1}H-^{15}N$ HSQC spectra of PLAAT3 and PLAAT4 were assigned using BMRB entries 16883 and 18012, respectively.[47,48]

Relaxation Dispersion Measurements. Constant relaxation time CPMG experiments were performed for the backbone ^{15}N nuclei of PLAAT3 and PLAAT4 using a modified ST-CW CPMG pulse sequence.[49] A series of two-dimensional (2D) spectra with 1024/60 complex points ($^{1}H/^{15}N$) were recorded with a relaxation delay (T_{relax}) of 40 ms and cpmg frequencies (Hz) set to 100, 200 (2×), 300, 400 (2×), 500, 600, 700, 800 (2×), 900, and 1000, run in an interleaved fashion, followed by a reference spectrum with $T_{relax} = 0$. Duplicates (2×) were used to estimate the error in the effective transverse relaxation rate ($R_{2,eff}$). Peaks were fitted with FuDa (Hansen, http://www.biochem.ucl.ac.uk/hansen/fuda/) to obtain intensities, and $R_{2,eff}$ values were calculated from the peak intensities using the formula: $R_{2,eff}(\nu_{CPMG}) = -1/T_{relax} \cdot \ln(I(\nu_{CPMG})/I_0)$, where I_0 is the peak intensity in the reference spectrum. The $R_{2,eff}$ values were corrected for R_1 contribution using the formula described by Jiang et al.[49] with 0.95 and 10.5 s^{-1} as an estimate for R_1 and R_2 contribution for all residues. The resulting relaxation dispersion profiles of residues that show dispersion obtained at two fields were fitted to Carver-Richards equation and modeled to a two-state model by using CATIA (Hansen, http://www.biochem.ucl.ac.uk/hansen/catia/), and the exchange rate constant (k_{ex}) and the fraction of the minor state (p_B) were obtained as the global output of CATIA, whereas the absolute chemical shift

https://doi.org/10.1021/acs.biochem.0c00974
Biochemistry 2021, 60, 1178−1190

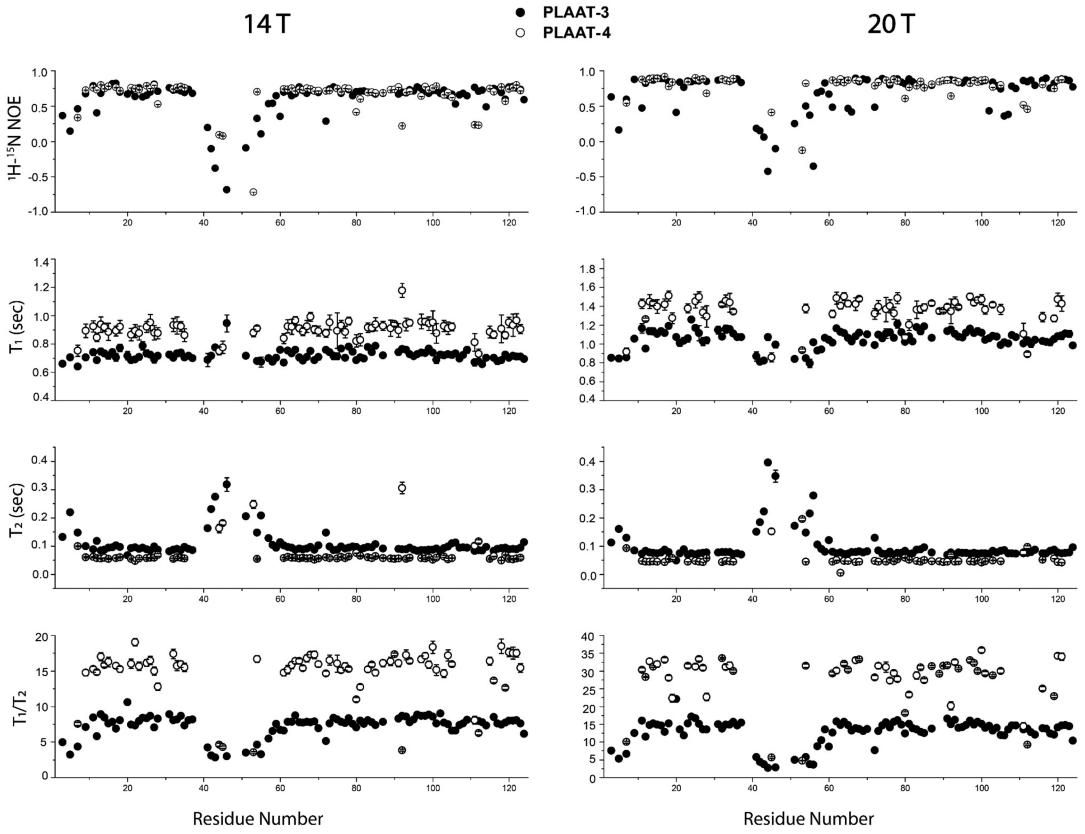

Figure 2. ^{15}N relaxation data for PLAAT3 (solid circles) and PLAAT4 (open circles) at 14 and 20 T. The ^{15}N-NOE, ^{15}N-T_1, and ^{15}N-T_2 as well as T_1/T_2 are plotted against the residue number. Errors were estimated by the Monte Carlo method using 95% confidence level as incorporated in the Bruker Protein Dynamics software suite.

differences between minor and major states ($|\Delta\omega|$) were obtained for individual residues.

Model-Free Analysis. Automated model-free analysis was performed using Bruker Protein Dynamics software suite. The NH bond length was set to 1.02 Å, and the NH chemical shift anisotropy was set to −172 ppm. To ensure good model fitting, calculated errors in T_1, T_2, and NOE were overridden with an error of 2%, as the calculated errors were smaller due to very high signal-to-noise. The software performs the following actions: Using the two-field T_1, T_2, and NOE data sets, the global correlation time (τ_c) and reduced spectral densities j(0), j(ω_N), j(0.87ω_H) were calculated. The reduced spectral densities were then used to estimate the order parameters (S^2), the ratio $D_{\parallel}/D_{\perp}$ of the diffusion tensor, and relaxation exchange (R_{ex}) parameters for each residue. Estimation of τ_c required exclusion of dynamic residues, which was done by excluding all residues with NOE values less than 0.65 residues, with T_2 smaller than the difference between mean and one standard deviation and with large T_2 values as compared to T_1 because these residues might undergo conformational exchange. The T_1, T_2, and NOE values of each residue were fitted to two models, assuming isotropic modeling: M1(S^2) and M2(S^2, τ_e).[50−55]

Theoretical Calculation of τ_c. Theoretical hydrodynamic calculation to determine the τ_c was done using the program HYDRONMR.[56] The structures from PDB entries 2KYT and 2MY9 were used as input for atomic coordinates. The effective radius of atomic elements was set to 3.1 Å, the temperature to 25 °C, and solvent viscosity to 9.1 mP to match our experimental conditions. N−H bonds with explicit hydrogens were chosen as the source of the dipole vectors to calculate the NMR parameters and dipolar couplings. The gyromagnetic ratio of N was set to -2.7126×10^7 rad s^{-1}T^{-1}, the N−H distance was set to 1.02 Å, and the CSA was set to −172 ppm. τ_c was calculated for two magnetic fields, 14 and 20 T to match our experimental data.

MD Simulations. MD simulations were performed using Gromacs-5.1.[57,58] The NMR structures of PLAAT3 (2KYT)[8] and PLAAT4 (2MY9)[7] were selected for the simulations as starting structures and topology files were created. The AMBER ff99sb-ILDN force-field provided with GROMACS was used.[59] The models were then solvated in a periodic water box of 10 and 20 Å cubic edge length for PLAAT3 and PLAAT4, respectively. The latter is larger due to the elongated conformation of the protein. The TIP3P water model was used.[60,61] Three Na^+ counterions were automatically placed by the GROMACS program throughout the water box such that the final system had net zero charge. The systems were energy minimized by 5000 steps of minimization using the steepest descent algorithm and further equilibrated under NVT and NPT conditions for 500 ps with a step size of 2 fs, using position restraints on the protein and a temperature of 27 °C and 1 atm pressure controlled by the velocity rescaling (modified Berendsen) thermostat[62] and Parrinello−Rahman barostat.[63] The equilibrated systems were subjected to a 100 ns simulation run under NPT without any position restraints, and coordinates were saved after every picosecond. Two simulations were carried out with different starting seeds for both PLAAT3 and PLAAT4, where each seed represents a simulation at a different velocity. The trajectories were

https://doi.org/10.1021/acs.biochem.0c00974
Biochemistry 2021, 60, 1178−1190

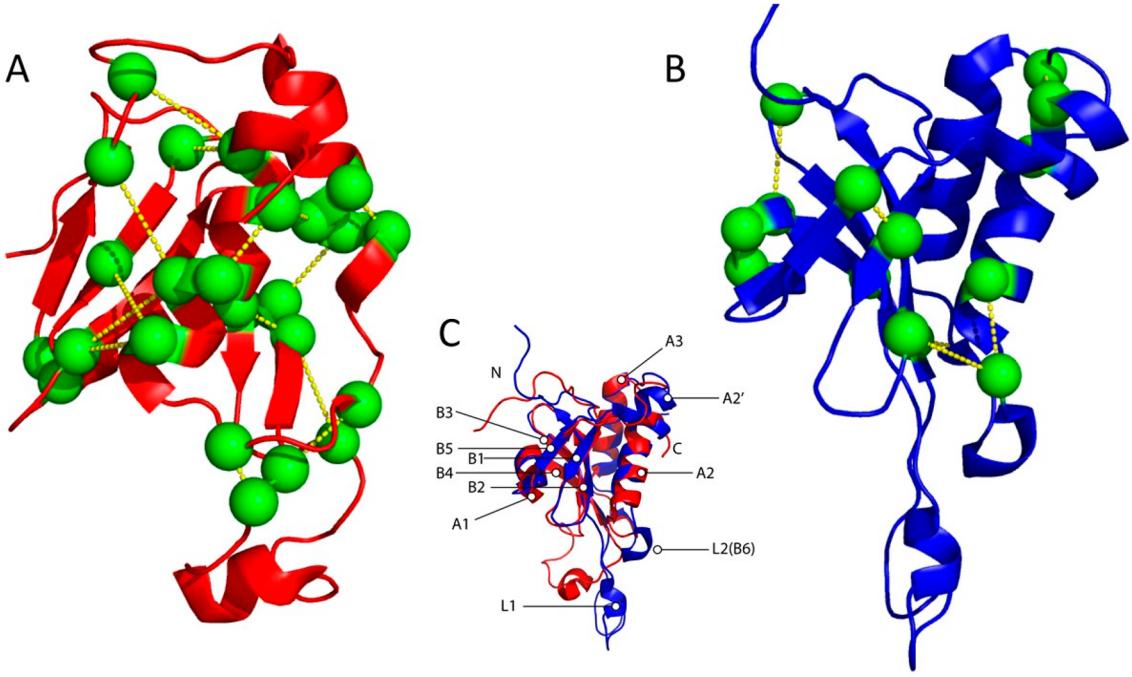

Figure 3. Representation of salt bridge networks (yellow dashes) in PLAAT3 (PDB ID: 2KYT) (A)[8] and PLAAT4 (PDB ID: 2MY9) (B).[7] Salt bridges were defined as a pair of basic and acidic residues with a nitrogen and an oxygen atom of the basic and acidic side chains, respectively, within 3.2 Å in at least one of the 20 NMR structures. Green spheres represent the Cα atoms of the bridged residues. (C) Modified nomenclature of PLAAT3 (red, PDB ID: 2KYT) and PLAAT-4 (blue, PDB ID: 2MY9) according to Table S2 is included for reference.

Table 1. 20% trimmed average and standard deviation in brackets of ^{15}N T_1, T_2, and NOE values of PLAAT3 and PLAAT4 obtained at 14 and 20 T experiments. The rotational correlation time τ_c for PLAAT3 (4) was calculated using subsets of 40 (33) or 57 (37) amides at 14 and 20 T, respectively

	14 T			20 T		
	T_1 (ms)	T_2 (ms)	NOE	T_1 (ms)	T_2 (ms)	NOE
PLAAT3						
20% trimmed mean	720(2)	90(1)	0.66(0.01)	1060(5)	80(2)	0.78(0.02)
τ_c (ns)	8.5(0.2)			8.2(0.4)		
PLAAT4						
20% trimmed mean	900(4)	50(8)	0.71(0.01)	1380(10)	40(1)	0.83(0.01)
τ_c (ns)	12.6(0.3)			12.5(0.4)		

analyzed using the in-built modules available in the GROMACS suite and visualized by means of the VMD[64]/Chimera program.[65]

Principal component analysis was carried out by first building the covariance matrix of atomic fluctuations and then generating a set of eigenvectors and eigenvalues by the diagonalization of the covariance matrix. The two eigenvectors that corresponded to the two largest eigenvalues were chosen as the principal components describing most of the collective motions or essential dynamics. The residues involved in these two largest eigenvectors were extracted by using a cutoff of 2 Å RMS fluctuations of individual atoms described by the two eigenvectors using an in-house program. The motions of these residues were further analyzed by observing the MD trajectory.

In Silico Mutagenesis. L2(B6) loops were swapped between PLAAT3 and PLAAT4 by mutating the wild-type NMR structures with Chimera[65] and selecting the most favorable conformation for each mutated residue. Clashes were removed during energy minimization in Gromacs.[57]

Salt-Bridge Analysis. Two MD simulations of 100 ns of L2(B6) mutant PLAATs were run using the same protocol as described above. Salt bridge populations were calculated for both wild-type and mutant proteins using VMD[64] by sampling a structure every 10 ps. The data were extracted and analyzed using an in-house written python program. Only residue pairs with salt bridges having populations of 20% or more, averaged over both runs, were taken into consideration.

RESULTS

PLAAT4 is Inherently More Flexible than PLAAT3. In the remaining, PLAAT3 and PLAAT4 refer to the truncated, NTD versions of the proteins. To characterize the differences in dynamics between PLAAT3 and PLAAT4, the melting temperature (T_m) and the mobility on various time scales were determined. The T_m values were found to be 78.0 (±0.5) °C for PLAAT3 and 62.5 (±0.5) °C for PLAAT4. The large difference of 15 °C suggests that PLAAT3 has a more rigid structure with strong inter-residue, noncovalent interactions. ^{1}H−^{15}N HSQC spectra of PLAAT3 and PLAAT4 were obtained and assigned based on the published data (Figure S1).[47,48] Fewer resonances are observed in the spectrum of PLAAT4 than in that of PLAAT3, which suggests that more

https://doi.org/10.1021/acs.biochem.0c00974
Biochemistry 2021, 60, 1178−1190

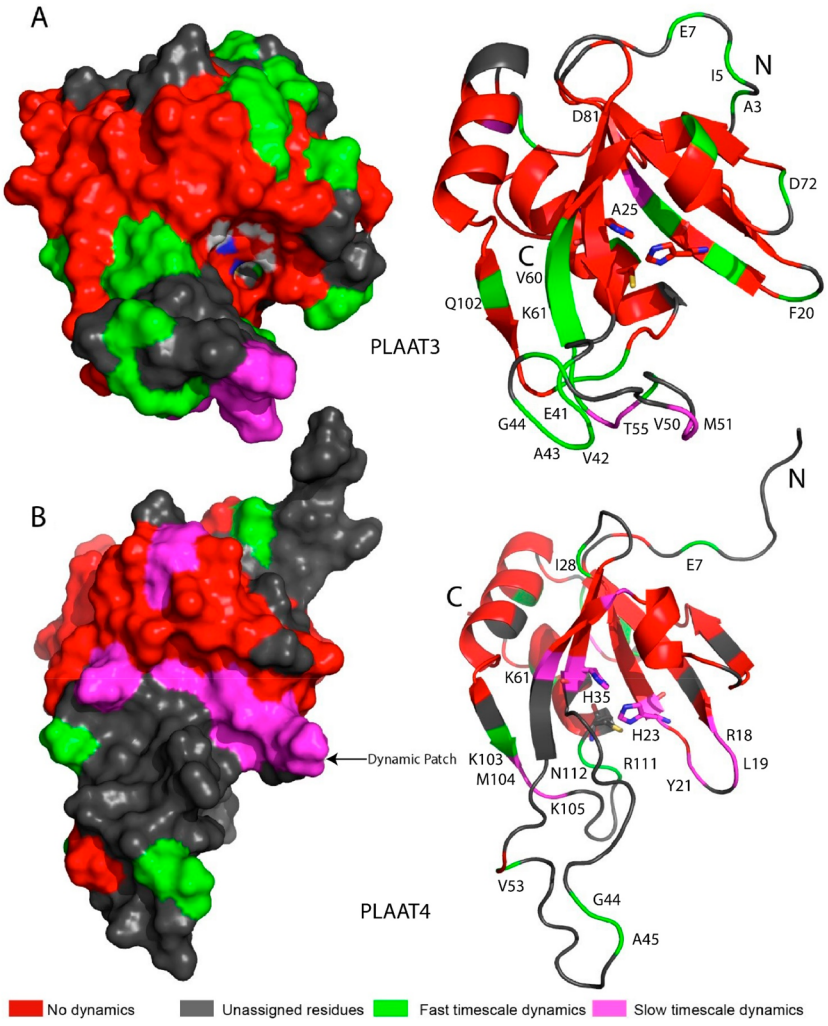

Figure 4. NMR-based analysis of mobility. Dynamics profiles mapped on the structures of PLAAT3 (A), PDB ID: 2KYT,[8] and PLAAT4 (B), PDB ID: 2MY9.[7] Unassigned residues are shown in gray, residues showing neither fast nor slow time scale motions are shown in red, residues showing only slow time scale dynamics are in pink, and residues showing only fast time scale dynamics are shown in green. Residues in fast or slow time scale motions are labeled. The dynamic patch present in PLAAT4 that includes the catalytic triad residues H23 and H35 is labeled.

amides are mobile on the millisecond time scale or their protons are in rapid exchange with the solvent, causing line broadening due to chemical exchange. To determine the motions of PLAAT3 and PLAAT4 at pico-/nanosecond time scale, the ^{15}N backbone amide T_1, T_2, and heteronuclear NOE parameters were determined at 14 T (600 MHz ^{1}H frequency) and 20 T (850 MHz ^{1}H frequency). The data are presented in Figure 2 and Tables S3−S6.

Relaxation parameters could be determined for 98 residues of PLAAT3 and 71 residues of PLAAT4. The low NOE values of the loop L1 in both proteins indicate that this loop is highly disordered, which is in line with previous findings.[2,7,8] Note that we have introduced minor modifications to the naming conventions of the secondary structural elements of PLAAT3 and PLAAT4 published in refs 7 and 8 (Table S2, Figure 3C). We have included the nomenclature for two main loops L1 (residues 38−57) and L2 (residue 100−109/110) and the β strand B6 (residues 103−104) as a part of the loop L2 and thus renamed as L2(B6). Due to the flexibility of the N-terminus and loop L1, the NOE and T_2 values of those regions differ much from the rigid parts of the proteins and should not be considered for the calculation of average T_1, T_2, and NOE values. The 20% trimmed average NOE and T_1 values for PLAAT4 were higher than for PLAAT3, and the one for T_2 was lower (Table 1).

Thus, the T_1/T_2 ratio is much larger for PLAAT4 than for PLAAT3, resulting in rotational correlation times (τ_c) of 8.4 and 12.5 ns for PLAAT3 and PLAAT4, respectively. This is remarkable, because the proteins have similar molecular weights, of 14.4 kDa and 14.7 kDa, respectively. Theoretical estimations of average τ_c from all models in the NMR ensemble structures (2kyt.pdb[8] for PLAAT3 and 2my9.pdb[7] for PLAAT4) using HYDRONMR[56] yield 9 ± 1 and 11 ± 1 ns, respectively, values close to experimentally determined ones. PLAAT3 is more globular with a compact structure, perhaps due to a distributed network of 17 salt bridges, whereas PLAAT4 is a more elongated molecule with only 10 salt bridges, concentrated in certain parts of the protein, as illustrated in Figure 3. It can also not be excluded that PLAAT4 has a tendency for transient self-interactions under the high concentration (1.5 mM) used in the NMR samples, leading to a higher τ_c. Residues with NOE values below two standard deviations of the trimmed average were identified as residues showing internal motions and residues with T_1/T_2 ratios two standard deviations above or below the trimmed mean were identified as exhibiting additional motion. The

https://doi.org/10.1021/acs.biochem.0c00974
Biochemistry 2021, 60, 1178−1190

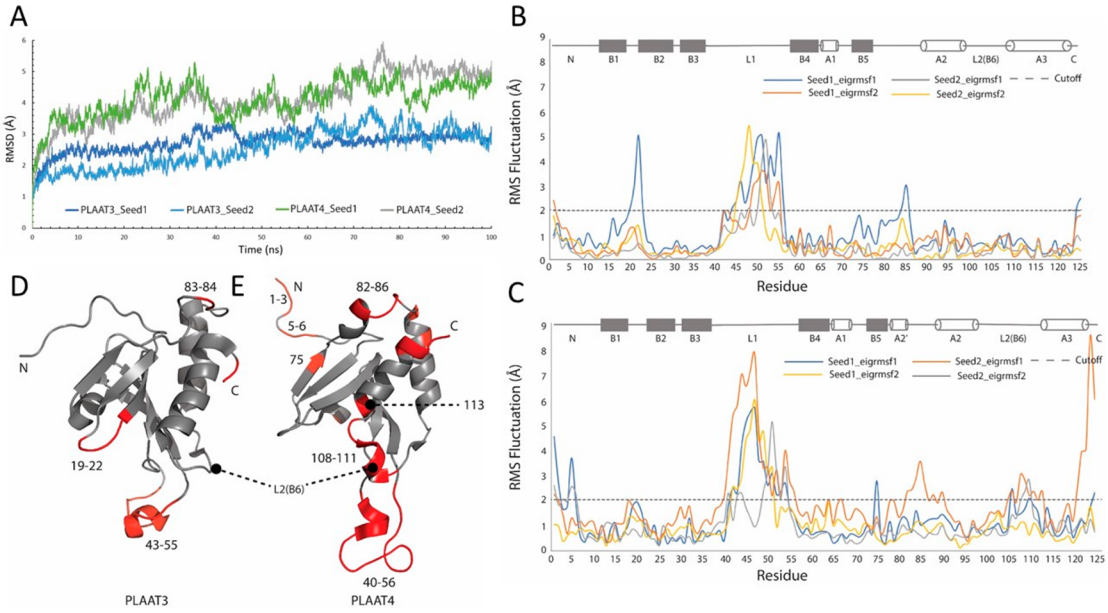

Figure 5. Molecular dynamics simulations of PLAAT3 and PLAAT4. (A) Plot of all-atom RMSD. Each point represents a snapshot saved at every picosecond. PLAAT4 shows a higher RMSD, suggesting significant conformational fluctuations and rearrangements with respect to the starting structure. (B, C) Fluctuations per residue. For each residue, the largest RMS fluctuation of all its atoms along the two largest eigenvectors (denoted as Seed1_eigrmsf1 and Seed2_eigrmsf2) of the principal component analysis in the MD runs is plotted for PLAAT3 (B) and PLAAT4 (C). A cutoff of 2 Å is indicated with a dashed line. Secondary structure of the starting structure is indicated at the top and named as in Table S2. (D, E) Results of principal component analysis of the MD simulations. Residues colored in red in PLAAT3 (D) and PLAAT4 (E) show RMS fluctuations above the cutoff of 2 Å. Apart from the C terminus, two distinct regions in PLAAT3 (19−22 and 43−55) were observed having concerted motions, bringing them closer, while rest of the protein stays relatively rigid. PLAAT4 has three distinct mobile regions apart from the N and the C termini. Loop L1 shows disordered movement, whereas regions 108−111 and 82−86 and residue 113 all show correlated motions.

residues demonstrating fast time scale (ps/ns) dynamics are mapped on the structures of both proteins (Figure 4). Also, residues for which resonances are not found in the spectra are indicated, as these are likely to be involved in motions or exchange processes. The Lipari−Szabo model-free approach[50,66] was used to derive the order parameters (S^2) of the backbone amides from the ^{15}N relaxation data. These are reported in the Supporting Information, Tables S7 and S8 and Figure S2.

To probe backbone motions in the slow (millisecond) time scale, we acquired ^{15}N-CPMG relaxation dispersion experiments[49] for both proteins at 14 and 20 T. Five residues of PLAAT3 showed weak relaxation dispersion (Figure S3). Three residues (V50, M51 and D56) are in the highly disordered loop L1, one residue (D81) in the loop joining B5 and A2 and another residue (W24) is in B2 (Figures 4 and S3). In contrast, 12 residues of PLAAT4 showed evidence for millisecond dynamics (Figures 4 and S4). PLAAT4 has a dynamic region consisting of 6 residues, R18, L19, Y21, K61 and the catalytic triad members H23 and H35. No resonance could be assigned to C113, the catalytic cysteine. The relaxation data of this region were fitted globally to a two-site exchange model, yielding a population (p_B) of 1% for the minor state and an exchange rate (k_{ex}) of 1.9 (0.2) × $10^3 s^{-1}$. Dynamic parameters of residues in both PLAAT3 and PLAAT4 are listed in Table S9.

To complement our insights from NMR studies and to obtain dynamics information on PLAAT3 and PLAAT4, classical all-atom MD simulations were performed using NMR structures solvated in a cubic water box, neutralized by counterions, and using the AMBERff99sb-ILDN force-field.[59] Two runs of 100 ns were performed with different starting velocities for both PLAAT3 and PLAAT4. The root-mean-square deviation (RMSD) of the structural snapshots as compared to the starting structure was taken as an indicator of the global conformational stability of a structure during the simulation (Figure 5A). In the first 10 ns, the RMSD steadily increases as the protein samples different conformations. The large RMSD observed for PLAAT4, as compared to that of PLAAT3, indicates that considerable structural fluctuations are taking place over the course of the simulations. The radius of gyration fluctuated around a value that remained stable during the MD simulations, with average values of 1.45 and 1.54 nm for PLAAT3 and PLAAT4, respectively (Figure S6).

RMS fluctuations were calculated for all residues globally (Figure S5) and also for the top two eigenvectors of the principal component to study essential dynamics (concerted motions). Residues with the highest RMS fluctuations of any atom above 2 Å (Figure 5, panels B and C) were plotted on the structures (Figure 5, panels D and E).

The regions showing major concerted fluctuations are similar for PLAAT3 and PLAAT4, and are localized in the termini, the major loop L1 and smaller loops. The main difference is observed for loop L2(B6). In PLAAT4, this loop shows concerted motions that are not observed in PLAAT3. The amide NMR resonances in this PLAAT4 loop are partly broadened beyond detection and partly involved in fast or slow dynamics (Figure 4), evidence that indeed this loop is dynamic. It is next to the area that was assigned as the dynamic patch on the basis of millisecond dynamics (Figure 4B). In PLAAT3, the distances between the active site atoms C113S$_\gamma$ and H23N$_\delta$ and between H23N$_\varepsilon$ and H35N$_\delta$ all remained below 5 Å (Figure S7), indicating that the active site triad remained intact over the course of the MD runs. In

https://doi.org/10.1021/acs.biochem.0c00974
Biochemistry 2021, 60, 1178−1190

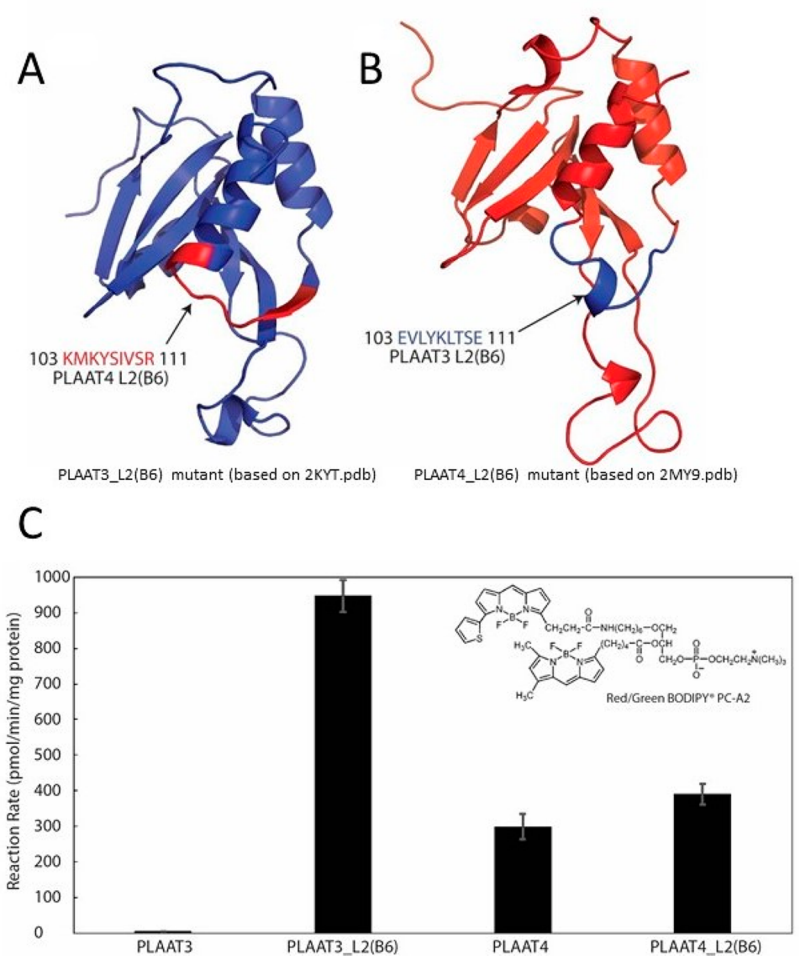

Figure 6. Models of mutants of PLAAT3-L2(B6)$_4$ (A) and PLAAT4-L2(B6)$_3$ (B). The mutated regions are shown in contrasting colors. (C) Phospholipase assay with Red/Green BODIPY PC-A2 (inset). The activity toward Red/Green BODIPY PC-A2 is plotted for PLAAT wild-type and loop mutants.

PLAAT4, C113S$_\gamma$ exhibited an RMS fluctuation of 2.3 Å, while its backbone atoms were more rigid (Figure 5C). The rearrangement of loop L2(B6) caused disruption of the interaction between the C113S$_\gamma$ and the histidine rings of the catalytic triad because the α-helix A3, of which C113 is a part, is connected to this loop (Figure 5C). We conclude that the L2(B6) motions, being interlinked with the interactions in the active site, could influence the activity of the enzyme.

Loop Exchange Strongly Enhances PLAAT3 Activity. To probe whether the mobility of L2(B6) affects the activity, the L2(B6) loops of PLAAT3 and PLAAT4 (residues 103−111) were exchanged (Figure 6). The mutants were named PLAAT3_L2(B6)$_4$ and PLAAT4_L2(B6)$_3$.

To test whether the hybrid enzymes were catalytically active and to establish the turnover rates, a phospholipase assay was performed with the fluorescent substrate Red/Green BODIPY PC-A2 (Figure 6C). The reaction rate of wild-type PLAAT4 was high, whereas wild-type PLAAT3 had background activity, in line with earlier studies.[2] Interestingly, PLAAT3_L2(B6)$_4$ shows a large increase in the reaction rate. This observation suggests that either the natural L2(B6)$_3$ in PLAAT3 was inhibiting the activity or that L2(B6) of PLAAT4 enables activity. For PLAAT4_L2(B6)$_3$, a small increase in activity was seen, as compared to wild-type PLAAT4. Thus, replacement of L2(B6)$_3$ with L2(B6)$_4$ in PLAAT3 enables activity, whereas the opposite mutation does not inhibit activity in PLAAT4.

L2(B6)$_4$ Disrupts Salt Bridges in PLAAT3. MD calculations on the loop-swapped mutants did not yield clear differences in dynamics between the wild-type proteins and the mutants when analyzing the RMSD (Figure S8) or concerted motions (Figures S9 and S10). As another measure of structural integrity, the presence of salt bridges during the MD run was analyzed. The presence of salt bridges was sampled every 10 ps over the entire MD trajectory and considered significant if the interaction was present on average over 2 runs for at least 20% of the time. Surprisingly large differences were found between wild-type and loop mutants. In wild-type PLAAT3, 11 salt bridges were identified (Table S10, Figure 7), whereas in PLAAT3_L2(B6)$_4$, only five of these remained. The lost interactions involved residues in the L2(B6) loop but also across the active site and even at the other end of the protein. Residues that lose the salt bridges found in the wild-type protein form new ones with other charged residues (Table S10, salt bridge pairs 12−15). A similar picture arises from the data of PLAAT4. Out of seven salt bridges in wild-type PLAAT4, only three were found in PLAAT4_L2(B6)$_3$ (Table S11, Figure 7). The lost bridges are in the L2(B6) loop, the active site, and around D81, at the other end of the protein. Only one new salt bridge was found in PLAAT4_L2(B6)$_3$. It is concluded that, despite the lack of changes in the overall and loop RMSD, the average structures clearly differ in details between wild-type and loop mutants.

https://doi.org/10.1021/acs.biochem.0c00974
Biochemistry 2021, 60, 1178−1190

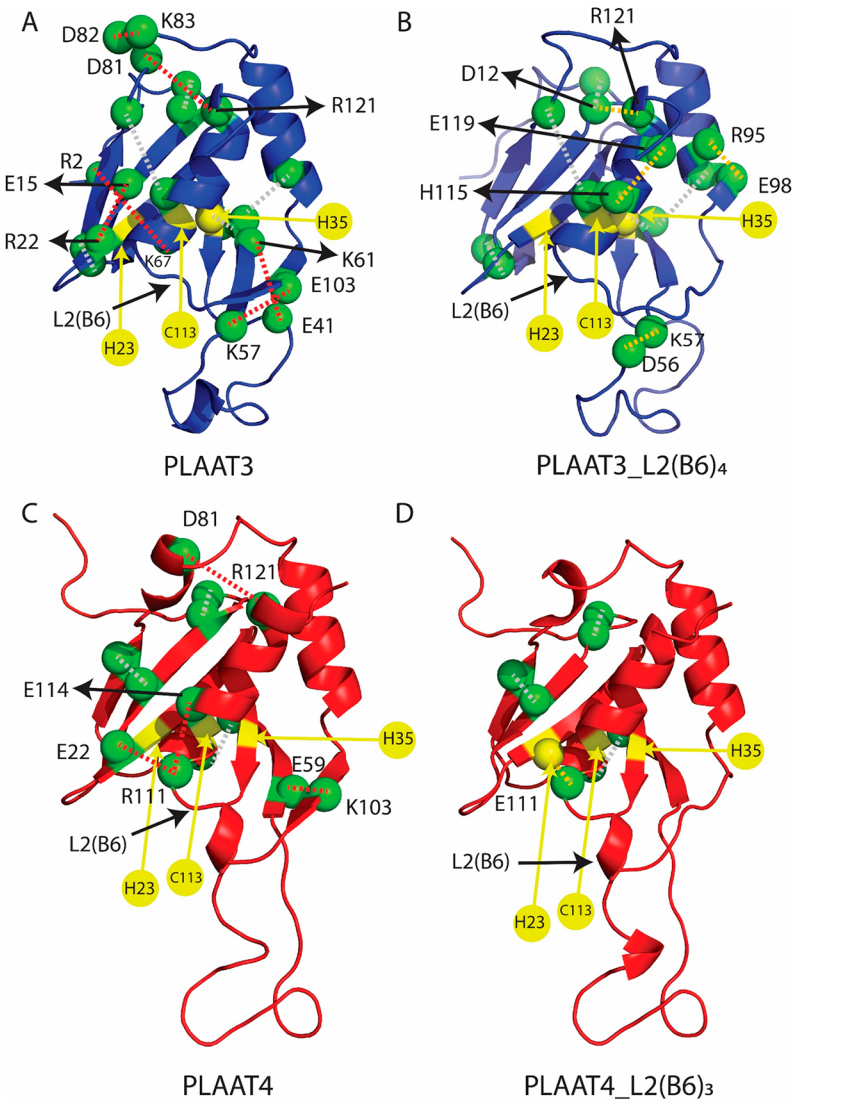

Figure 7. Salt bridges in wild-type and loop mutant PLAAT proteins. Residues involved in salt bridges with an average occupancy of at least 20% in the two 100 ns MD runs are shown with green spheres for Cα atoms. Dashed lines indicate the presence of salt bridges between the side chains of the connected residues in wild-type only (red), wild-type and mutant (gray), or mutant only (yellow) for PLAAT3 (A), PLAAT3_L2(B6)$_4$ (B), PLAAT4 (C), and PLAAT4_L2(B6)$_3$ (D). The residues of the catalytic triad are marked in yellow.

DISCUSSION

We aimed to study the reason for activity differences between the homologous enzymes PLAAT3 and PLAAT4. We hypothesized that differences in dynamics could play a role on the basis of observations accumulating over the years on the role of C-terminal (CTD) and N-terminal domains of these proteins. The transmembrane CTD was found to be crucial for PLAAT3 PLA$_{1/2}$ activity. Uyama et al.[45] showed that removal of this domain resulted in loss of phospholipase activity. In contrast, Golczak et al.[2] demonstrated that PLAAT4 truncated to its NTD has phospholipase activity, indicating that the transmembrane C-terminal domain is not critical. Golczak et al. also demonstrated that the rate of hydrolysis of short chain phosphatidylcholines of NTD of PLAAT4 is faster than the NTD of PLAAT3. Xia et al.[7] reported that C-terminal domains (CTDs) of both PLAAT4 and PLAAT3 can induce HeLa cell death at a comparable level, while their NTDs play opposite roles in regulating the cell death activity, even though their structures are highly similar. The NTD of PLAAT4 was found to be enhancing the cell death effect of the CTD, whereas the NTD of PLAAT3 was found to be inhibitory. These authors also complemented the observations of a previous study by Scharadin et al.[67] who found that residues 102−125, part of the loop we renamed as L2(B6), of full-length PLAAT4 was necessary for pericentrosomal localization. Based on NMR studies, Wei et al.[7] hypothesized that the motif (residues 102−125) in PLAAT3 might be covered by the CTD while it was exposed in PLAAT4. Therefore, we hypothesized that there must lie a connection between the activities and overall dynamics contributed by amino acid differences between PLAAT3 and PLAAT4 NTDs and especially loop L2(B6).

The melting temperature of PLAAT3 is 15 °C higher than that of PLAAT4, and the rotational correlation time is 33% shorter, showing that in solution PLAAT3 is a more stable and compact protein than PLAAT4. A comparison of the salt bridge networks show that the former has a more extensive network of salt bridges, which could explain these observations. Both proteins feature a large loop (L1) that is known to be disordered[2,7,8,68] and is shown here to be mobile on the pico-/

https://doi.org/10.1021/acs.biochem.0c00974
Biochemistry 2021, 60, 1178−1190

nanosecond time scale. It has been proposed that L1 is a membrane anchoring loop in the full length protein.[68] It was shown that replacement of L1 in PLAAT3 by the equivalent loop of LRAT leads to induction of Vitamin A conversion.[68] This indicates that the highly disordered loop may play a role in modulating activity by interacting with the membrane. Interesting differences are found between PLAAT3 and PLAAT4 around the active site. PLAAT4 shows low order parameters for R111 and N112, which immediately precede the catalytic nucleophile C113. Because there are no NMR resonance assignments for residues 106−110 and 113−114 in PLAAT4, we assume that the peaks of these residues are lacking because of line broadening due to motional chemical exchange. Millisecond time scale dynamics experiments identified a dynamic active site region involving residues 18, 19, 21, 23, 35, and 61. The resonance of G20 is missing, again indicative of exchange broadening. Residue E22, which forms a salt bridge with R111, shows no broadening due to chemical exchange, which could imply that it either is not dynamic or its change in chemical shift ($\Delta\omega$) happens to be small. Thus, the active site region of PLAAT4 is dynamic, involving at least residues 18−23, 35, 61, and also 113−114. Such a dynamic patch is not observed in PLAAT3. We speculated that the difference in dynamics can explain the activity differences observed PLAAT3 and PLAAT4. The NTD of PLAAT3 may show little activity toward its substrate due to lack of active site dynamics, whereas the dynamics of PLAAT4 may enable its activity. To develop a model of what the dynamics in PLAAT4 may entail, molecular dynamics simulations were used. Although they can only sample fast dynamics, they still provided insight into the nature of motions, and such calculations are known to correlate with NMR relaxation studies.[69−72] The RMSD profiles obtained from the MD simulations indicated that PLAAT4 is inherently more dynamic than PLAAT3, supporting the NMR results. Using PCA, we also demonstrated that the loop L2(B6) in PLAAT4 shows concerted motions that are absent in PLAAT3.

Thus, these observations raised the question whether the mobility of L2(B6) relates to the activity difference between PLAAT3 and PLAAT4. Increased flexibility could play a role in substrate accessibility or induced fit. Introduction of the PLAAT4 L2(B6) loop indeed increased the activity of PLAAT3 strongly, though the opposite change, introducing L2(B6) from PLAAT3 into PLAAT4, did not reduce activity. By studying the lifetimes of the salt bridges during MD simulations of L2(B6)-swapped structures, we could observe that the introduction of a non-native L2(B6) disrupts the inherent network of salt bridges, the disruption being more prominent in PLAAT3, reducing some of the structural rigidity which might enhance activity of PLAAT_L2(B6)$_4$, perhaps by increasing substrate accessibility or greater active site flexibility.

Apart from L2(B6), studying the interaction between L2(B6) and the highly flexible loop L1 in modulating catalytic activity (especially for PLAAT3) is another facet to a greater understanding of the workings of these enzymes because the two loops are adjacent to each other in NTD structures. However, in light of the models proposed by Golczak et al.[2] and Pang et al.[23] for full-length enzymes, the two loops are expected to be far apart when interacting with the membrane. Wei et al.[7] show that deletion of L1 in PLAAT3 enhances cell death inducing ability, not necessarily the phospholipase activity, because cell death inducing ability is conferred by the C-terminal domain. The authors mention that it is still not clear whether phospholipase activity plays any role in cell death. Therefore, the role of loop L1 in modulating phospholipase activity of PLAAT3 is unclear. We tried to address the question of interaction between loops L1 and L2(B6) in the NTD. Studying the interaction using NMR spectroscopy poses challenges because the NH resonances of the residues constituting L1 are broadened beyond detection. The MD simulations show no evidence for contacts. The C_α distances between two pairs of residues in L2(B6) and L1 [Q102 and L105/K105 (PLAAT3/PLAAT4) in L2(B6) and A45 and V50 in L1] were calculated over the MD trajectory (Figure S11). The two loops, however flexible, do not interact significantly with each other.

Based on our findings, it can be concluded that PLAAT3 and PLAAT4 are dynamic proteins and the motions involve large parts of the structure. These motions clearly play an important role in modulating the activity, making it hard to explain activity differences with a simple model. For complete structural understanding of the activity difference of PLAAT family members, it will be important to compare the dynamics of the NTDs with those of the full-length proteins in a seminative environment, such as a Nanodisc. Studying full-length proteins in Nanodiscs would also help decipher the role of the CTD and any possible interaction between the CTD and L1 loop because L1 also interacts with the membrane and therefore should assume more defined conformation than the highly flexible loop that is observed for the NTD. It would be interesting to see if the interaction of the CTD and L1 with the membrane bring about any conformational change or change in dynamics in the NTD of PLAAT3, thereby rendering it more catalytically active than NTD itself.

■ ASSOCIATED CONTENT

Supporting Information

The Supporting Information is available free of charge at https://pubs.acs.org/doi/10.1021/acs.biochem.0c00974.

> Alternative names for PLAAT proteins found in literature; modified nomenclature of the secondary structural elements of PLAAT3 and PLAAT4; relaxation parameters; S^2 and τ_e values; exchange parameters from relaxation disperion experiments; salt bridge analysis; HSQC spectra; relaxation dispersion curves; RMS fluctuations per residue; plot of radius of gyration; inter-residue heavy atom distances during the two runs of MD simulations; structural fluctuations on the nanosecond time scale; correlated motions across the active site; distance plots (PDF)

Accession Codes

PLAAT3: Uniprot ID P53816, PLAAT4: Uniprot ID Q9UL19.

■ AUTHOR INFORMATION

Corresponding Author

Marcellus Ubbink − *Leiden Institute of Chemistry, Leiden University, 2333 CC Leiden, The Netherlands;* orcid.org/0000-0002-2615-6914; Phone: +31 715274628; Email: m.ubbink@chem.leidenuniv.nl

Authors

Soumya Deep Chatterjee − *Leiden Institute of Chemistry, Leiden University, 2333 CC Leiden, The Netherlands*

Juan Zhou − *Leiden Institute of Chemistry, Leiden University, 2333 CC Leiden, The Netherlands*

Rubin Dasgupta − *Leiden Institute of Chemistry, Leiden University, 2333 CC Leiden, The Netherlands;* orcid.org/0000-0003-4505-7775
Anneloes Cramer-Blok − *Leiden Institute of Chemistry, Leiden University, 2333 CC Leiden, The Netherlands*
Monika Timmer − *Leiden Institute of Chemistry, Leiden University, 2333 CC Leiden, The Netherlands*
Mario van der Stelt − *Leiden Institute of Chemistry, Leiden University, 2333 CC Leiden, The Netherlands*

Complete contact information is available at: https://pubs.acs.org/10.1021/acs.biochem.0c00974

Funding
The study was supported by Netherlands Magnetic Resonance Research School (NWO-BOO 022.005.029).

Notes
The authors declare no competing financial interest.

■ ABBREVIATIONS
PLAAT, phospholipase A/acyltransferase; NAPE, *N*-acyl phosphatidyl ethanolamine; NAE, *N*-acylethanolamine; MD, molecular dynamics; NMR, nuclear magnetic resonance

■ REFERENCES
(1) Ito, H., Akiyama, H., Shigeno, C., and Nakamura, T. (2001) Isolation, characterization, and chromosome mapping of a human A-C1 Ha-Ras suppressor gene (HRASLS). *Cytogenet. Genome Res. 93*, 36−39.
(2) Golczak, M., Kiser, P. D., Sears, A. E., Lodowski, D. T., Blaner, W. S., and Palczewski, K. (2012) Structural basis for the acyltransferase activity of lecithin:retinol acyltransferase-like proteins. *J. Biol. Chem. 287*, 23790−23807.
(3) Jin, X.-H., Uyama, T., Wang, J., Okamoto, Y., Tonai, T., and Ueda, N. (2009) cDNA cloning and characterization of human and mouse Ca2+-independent phosphatidylethanolamine N-acyltransferases. *Biochim. Biophys. Acta, Mol. Cell Biol. Lipids 1791*, 32−38.
(4) Ruiz, A., Winston, A., Lim, Y.-H., Gilbert, B. A., Rando, R. R., and Bok, D. (1999) Molecular and biochemical characterization of lecithin retinol acyltransferase. *J. Biol. Chem. 274*, 3834−3841.
(5) Kiser, P. D., Golczak, M., Maeda, A., and Palczewski, K. (2012) Key enzymes of the retinoid (visual) cycle in vertebrate retina. *Biochim. Biophys. Acta, Mol. Cell Biol. Lipids 1821*, 137−151.
(6) Anantharaman, V., and Aravind, L. (2003) Evolutionary history, structural features and biochemical diversity of the NlpC/P60 superfamily of enzymes. *Genome Biol. 4*, R11−R11.
(7) Wei, H., Wang, L., Ren, X., Yu, W., Lin, J., Jin, C., and Xia, B. (2015) Structural and functional characterization of tumor suppressors TIG3 and H-REV107. *FEBS Lett. 589*, 1179−1186.
(8) Ren, X., Lin, J., Jin, C., and Xia, B. (2010) Solution structure of the N-terminal catalytic domain of human H-REV107–a novel circular permutated NlpC/P60 domain. *FEBS Lett. 584*, 4222−4226.
(9) Shyu, R.-Y., Hsieh, Y.-C., Tsai, F.-M., Wu, C.-C., and Jiang, S.-Y. (2008) Cloning and functional characterization of the HRASLS2 gene. *Amino Acids 35*, 129−137.
(10) Calignano, A., Rana, G. La, Giuffrida, A., and Piomelli, D. (1998) Control of pain initiation by endogenous cannabinoids. *Nature 394*, 277−281.
(11) Lambert, D., Vandevoorde, S., Jonsson, K.-O., and Fowler, C. (2002) The palmitoylethanolamide family: a new class of anti-inflammatory agents? *Curr. Med. Chem. 9*, 663−674.
(12) Rahman, I. A. S., Tsuboi, K., Uyama, T., and Ueda, N. (2014) New players in the fatty acyl ethanolamide metabolism OH OH OH. *Pharmacol. Res. 86*, 1−10.
(13) Rodríguez de Fonseca, F., Navarro, M., Gómez, R., Escuredo, L., Nava, F., Fu, J., Murillo-Rodríguez, E., Giuffrida, A., LoVerme, J., Gaetani, S., Kathuria, S., Gall, C., and Piomelli, D. (2001) An anorexic lipid mediator regulated by feeding. *Nature 414*, 209−212.
(14) Devane, W. A., Hanus, L., Breuer, A., Pertwee, R. G., Stevenson, L. A., Griffin, G., Gibson, D., Mandelbaum, A., Etinger, A., and Mechoulam, R. (1992) Isolation and structure of a brain constituent that binds to the cannabinoid receptor. *Science (80-.). 258*, 1946LP−1949.
(15) Di Marzo, V. (1998) 'Endocannabinoids' and other fatty acid derivatives with cannabimimetic properties: biochemistry and possible physiopathological relevance. *Biochim. Biophys. Acta, Lipids Lipid Metab. 1392*, 153−175.
(16) Di Marzo, V., De Petrocellis, L., Fezza, F., Ligresti, A., and Bisogno, T. (2002) Anandamide receptors. *Prostaglandins, Leukotrienes Essent. Fatty Acids 66*, 377−391.
(17) Shinohara, N., Uyama, T., Jin, X., Tsuboi, K., Tonai, T., Houchi, H., and Ueda, N. (2011) Enzymological analysis of the tumor suppressor A-C1 reveals a novel group of phospholipid-metabolizing enzymes. *J. Lipid Res. 52*, 1927−1935.
(18) Jin, X.-H., Okamoto, Y., Morishita, J., Tsuboi, K., Tonai, T., and Ueda, N. (2007) Discovery and characterization of a Ca2+-independent phosphatidylethanolamine N-acyltransferase generating the anandamide precursor and its congeners. *J. Biol. Chem. 282*, 3614−3623.
(19) Uyama, T., Jin, X.-H., Tsuboi, K., Tonai, T., and Ueda, N. (2009) Characterization of the human tumor suppressors TIG3 and HRASLS2 as phospholipid-metabolizing enzymes. *Biochim. Biophys. Acta, Mol. Cell Biol. Lipids 1791*, 1114−1124.
(20) Hajnal, A., Klemenz, R., and Schäfer, R. (1994) Subtraction cloning of H-rev107, a gene specifically expressed in H-ras resistant fibroblasts. *Oncogene 9*, 479−490.
(21) Duncan, R. E., Sarkadi-Nagy, E., Jaworski, K., Ahmadian, M., and Sul, H. S. (2008) Identification and functional characterization of adipose-specific phospholipase A2 (AdPLA). *J. Biol. Chem. 283*, 25428−25436.
(22) Uyama, T., Morishita, J., Jin, X.-H., Okamoto, Y., Tsuboi, K., and Ueda, N. (2009) The tumor suppressor gene H-Rev107 functions as a novel Ca2+-independent cytosolic phospholipase A1/2 of the thiol hydrolase type. *J. Lipid Res. 50*, 685−693.
(23) Pang, X.-Y., Cao, J., Addington, L., Lovell, S., Battaile, K. P., Zhang, N., Rao, J. L. U. M., Dennis, E. A., and Moise, A. R. (2012) Structure/function relationships of adipose phospholipase A2 containing a Cys-His-His catalytic triad. *J. Biol. Chem. 287*, 35260−35274.
(24) Uyama, T., Ikematsu, N., Inoue, M., Shinohara, N., Jin, X.-H., Tsuboi, K., Tonai, T., Tokumura, A., and Ueda, N. (2012) Generation of N -acylphosphatidylethanolamine by members of the phospholipase A/acyltransferase (PLA/AT) family. *J. Biol. Chem. 287*, 31905−31919.
(25) Jaworski, K., Ahmadian, M., Duncan, R. E, Sarkadi-Nagy, E., Varady, K. A, Hellerstein, M. K, Lee, H.-Y., Samuel, V. T, Shulman, G. I, Kim, K.-H., de Val, S., Kang, C., and Sul, H. S. (2009) AdPLA ablation increases lipolysis and prevents obesity induced by high-fat feeding or leptin deficiency. *Nat. Med. 15*, 159−168.
(26) Sers, C., Emmenegger, U., Husmann, K., Bucher, K., Andres, A. C., and Schäfer, R. (1997) Growth-inhibitory activity and down-regulation of the class II tumor-suppressor gene H-rev107 in tumor cell lines and experimental tumors. *J. Cell Biol. 136*, 935−944.
(27) Roder, K., Latasa, M.-J., and Sul, H. S. (2002) Silencing of the mouse H-rev107 gene encoding a class II tumor suppressor by CpG methylation. *J. Biol. Chem. 277*, 30543−30550.
(28) Yanatatsaneejit, P., Chalermchai, T., Kerekhanjanarong, V., Shotelersuk, K., Supiyaphun, P., Mutirangura, A., and Sriuranpong, V. (2008) Promoter hypermethylation of CCNA1, RARRES1, and HRASLS3 in nasopharyngeal carcinoma. *Oral Oncol. 44*, 400−406.
(29) Nazarenko, I., Kristiansen, G., Fonfara, S., Guenther, R., Gieseler, C., Kemmner, W., Schafer, R., Petersen, I., and Sers, C. (2006) H-REV107−1 stimulates growth in non-small cell lung carcinomas via the activation of mitogenic signaling. *Am. J. Pathol. 169*, 1427−1439.

(30) Nazarenko, I., Schäfer, R., and Sers, C. (2007) Mechanisms of the HRSL3 tumor suppressor function in ovarian carcinoma cells. *J. Cell Sci. 120*, 1393LP−1404.
(31) Shyu, R.-Y., Wu, C.-C., Wang, C.-H., Tsai, T.-C., Wang, L.-K., Chen, M.-L., Jiang, S.-Y., and Tsai, F.-M. (2013) H-rev107 regulates prostaglandin D2 synthase-mediated suppression of cellular invasion in testicular cancer cells. *J. Biomed. Sci. 20*, 30.
(32) Wang, C.-H., Shyu, R.-Y., Wu, C.-C., Tsai, T.-C., Wang, L.-K., Chen, M.-L., Jiang, S.-Y., and Tsai, F.-M. (2014) Phospholipase A/Acyltransferase enzyme activity of H-rev107 inhibits the H-RAS signaling pathway. *J. Biomed. Sci. 21*, 36.
(33) Xiong, S., Tu, H., Kollareddy, M., Pant, V., Li, Q., Zhang, Y., Jackson, J. G., Suh, Y.-A., Elizondo-Fraire, A. C., Yang, P., Chau, G., Tashakori, M., Wasylishen, A. R., Ju, Z., Solomon, H., Rotter, V., Liu, B., El-Naggar, A. K., Donehower, L. A., Martinez, L. A., and Lozano, G. (2014) Pla2g16 phospholipase mediates gain-of-function activities of mutant p53. *Proc. Natl. Acad. Sci. U. S. A. 111*, 11145−11150.
(34) Scharadin, T. M., and Eckert, R. L. (2014) TIG3: an important regulator of keratinocyte proliferation and survival. *J. Invest. Dermatol. 134*, 1811−1816.
(35) Jans, R., Sturniolo, M. T., and Eckert, R. L. (2008) Localization of the TIG3 transglutaminase interaction domain and demonstration that the amino-terminal region is required for TIG3 function as a keratinocyte differentiation regulator. *J. Invest. Dermatol. 128*, 517−529.
(36) Sturniolo, M. T., Dashti, S. R., Deucher, A., Rorke, E. A., Broome, A.-M., Chandraratna, R. A. S., Keepers, T., and Eckert, R. L. (2003) A novel tumor suppressor protein promotes keratinocyte terminal differentiation via activation of type I transglutaminase. *J. Biol. Chem. 278*, 48066−48073.
(37) Sturniolo, M. T., Chandraratna, R. A. S., and Eckert, R. L. (2005) A novel transglutaminase activator forms a complex with type 1 transglutaminase. *Oncogene 24*, 2963−2972.
(38) DiSepio, D., Ghosn, C., Eckert, R. L., Deucher, A., Robinson, N., Duvic, M., Chandraratna, R. A., and Nagpal, S. (1998) Identification and characterization of a retinoid-induced class II tumor suppressor/growth regulatory gene. *Proc. Natl. Acad. Sci. U. S. A. 95*, 14811−14815.
(39) Huang, S.-L., Shyu, R.-Y., Yeh, M.-Y., and Jiang, S.-Y. (2000) Cloning and characterization of a novel retinoid-inducible gene 1(RIG1) deriving from human gastric cancer cells. *Mol. Cell. Endocrinol. 159*, 15−24.
(40) Casanova, B., de la Fuente, M. T., Garcia-Gila, M., Sanz, L., Silva, A., Garcia-Marco, J. A., and Garcia-Pardo, A. (2001) The class II tumor-suppressor gene RARRES3 is expressed in B cell lymphocytic leukemias and down-regulated with disease progression. *Leukemia 15*, 1521−1526.
(41) Tsai, F.-M., Shyu, R.-Y., and Jiang, S.-Y. (2007) RIG1 suppresses Ras activation and induces cellular apoptosis at the Golgi apparatus. *Cell. Signalling 19*, 989−999.
(42) Huang, S.-L., Shyu, R.-Y., Yeh, M.-Y., and Jiang, S.-Y. (2002) The retinoid-inducible gene I: effect on apoptosis and mitogen-activated kinase signal pathways. *Anticancer Res. 22*, 799−804.
(43) Morales, M., Arenas, E. J., Urosevic, J., Guiu, M., Fernández, E., Planet, E., Fenwick, R. B., Fernández-Ruiz, S., Salvatella, X., Reverter, D., Carracedo, A., Massagué, J., and Gomis, R. R. (2014) RARRES3 suppresses breast cancer lung metastasis by regulating adhesion and differentiation. *EMBO Mol. Med. 6*, 865−881.
(44) Duvic, M., Helekar, B., Schulz, C., Cho, M., DiSepio, D., Hager, C., DiMao, D., Hazarika, P., Jackson, B., Breuer-McHam, J., Young, J., Clayman, G., Lippman, S. M., Chandraratna, R. A. S., Robinson, N. A., Deucher, A., Eckert, R. L., and Nagpal, S. (2000) Expression of a retinoid-inducible tumor suppressor, tazarotene-inducible gene-3, is decreased in psoriasis and skin cancer. *Clin. Cancer Res. 6*, 3249LP−3259.
(45) Uyama, T., Kawai, K., Kono, N., Watanabe, M., Tsuboi, K., Inoue, T., Araki, N., Arai, H., and Ueda, N. (2015) Interaction of phospholipase A/acyltransferase-3 with Pex19p: a possible involvement in the down-regulation of peroxisomes. *J. Biol. Chem. 290*, 17520−17534.
(46) Heydenreich, F. M., Miljuš, T., Jaussi, R., Benoit, R., Milić, D., and Veprintsev, D. B. (2017) High-throughput mutagenesis using a two-fragment PCR approach. *Sci. Rep. 7*, 6787.
(47) Wang, L., Yu, W., Ren, X., Lin, J., Jin, C., and Xia, B. (2012) 1H, 13C, and 15N resonance assignments of the N-terminal domain of human TIG3. *Biomol. NMR Assignments 6*, 201−203.
(48) Ren, X., Lin, J., Jin, C., and Xia, B. (2010) 1H, 13C and 15N resonance assignments of human H-REV107 N-terminal domain. *Biomol. NMR Assignments 4*, 175−178.
(49) Jiang, B., Yu, B., Zhang, X., Liu, M., and Yang, D. (2015) A 15N CPMG relaxation dispersion experiment more resistant to resonance offset and pulse imperfection. *J. Magn. Reson. 257*, 1−7.
(50) Lipari, G., and Szabo, A. (1982) Model-free approach to the interpretation of nuclear magnetic resonance relaxation in macromolecules. 1. Theory and range of validity. *J. Am. Chem. Soc. 104*, 4546−4559.
(51) Clore, G. M., Szabo, A., Bax, A., Kay, L. E., Driscoll, P. C., and Gronenborn, A. M. (1990) Deviations from the simple two-parameter model-free approach to the interpretation of nitrogen-15 nuclear magnetic relaxation of proteins. *J. Am. Chem. Soc. 112*, 4989−4991.
(52) Orekhov, V. Y., Korzhnev, D. M., Diercks, T., Kessler, H., and Arseniev, A. S. (1999) 1H-15N NMR dynamic study of an isolated α-helical peptide (1−36)- bacteriorhodopsin reveals the equilibrium helix-coil transitions. *J. Biomol. NMR 14*, 345−356.
(53) Fushman, D., Cahill, S., and Cowburn, D. (1997) The main-chain dynamics of the dynamin pleckstrin homology (PH) domain in solution: analysis of 15N relaxation with monomer/dimer equilibration11Edited by P.E. Wright. *J. Mol. Biol. 266*, 173−194.
(54) Korzhnev, D. M., Billeter, M., Arseniev, A. S., and Orekhov, V. Y. (2001) NMR studies of Brownian tumbling and internal motions in proteins. *Prog. Nucl. Magn. Reson. Spectrosc. 38*, 197−266.
(55) Mandel, A. M., Akke, M., and Palmer, A. G., III (1995) Backbone dynamics of Escherichia coli ribonuclease HI: correlations with structure and function in an active enzyme. *J. Mol. Biol. 246*, 144−163.
(56) Garcıa de la Torre, J, Huertas, M.L, and Carrasco, B (2000) HYDRONMR: prediction of NMR relaxation of globular proteins from atomic-level structures and hydrodynamic calculations. *J. Magn. Reson. 147*, 138−146.
(57) Van Der Spoel, D., Lindahl, E., Hess, B., Groenhof, G., Mark, A. E., and Berendsen, H. J. C. (2005) GROMACS: Fast, flexible, and free. *J. Comput. Chem. 26*, 1701−1718.
(58) Hess, B., Kutzner, C., van der Spoel, D., and Lindahl, E. (2008) GROMACS 4: algorithms for highly efficient, load-balanced, and scalable molecular simulation. *J. Chem. Theory Comput. 4*, 435−447.
(59) Lindorff-Larsen, K., Piana, S., Palmo, K., Maragakis, P., Klepeis, J. L., Dror, R. O., and Shaw, D. E. (2010) Improved side-chain torsion potentials for the Amber ff99SB protein force field. *Proteins: Struct., Funct., Genet. 78*, 1950−1958.
(60) Jorgensen, W. L. (1981) Quantum and statistical mechanical studies of liquids. 10. Transferable intermolecular potential functions for water, alcohols, and ethers. Application to liquid water. *J. Am. Chem. Soc. 103*, 335−340.
(61) Mark, P., and Nilsson, L. (2001) Structure and dynamics of the TIP3P, SPC, and SPC/E water models at 298 K. *J. Phys. Chem. A 105*, 9954−9960.
(62) Bussi, G., Donadio, D., and Parrinello, M. (2007) Canonical sampling through velocity rescaling. *J. Chem. Phys. 126*, 14101.
(63) Parrinello, M., and Rahman, A. (1981) Polymorphic transitions in single crystals: A new molecular dynamics method. *J. Appl. Phys. 52*, 7182−7190.
(64) Humphrey, W., Dalke, A., and Schulten, K. (1996) VMD: Visual molecular dynamics. *J. Mol. Graphics 14*, 33−38.
(65) Pettersen, E. F., Goddard, T. D., Huang, C. C., Couch, G. S., Greenblatt, D. M., Meng, E. C., and Ferrin, T. E. (2004) UCSF Chimera—A visualization system for exploratory research and analysis. *J. Comput. Chem. 25*, 1605−1612.

https://doi.org/10.1021/acs.biochem.0c00974
Biochemistry 2021, 60, 1178−1190

(66) Lipari, G., and Szabo, A. (1982) Model-free approach to the interpretation of nuclear magnetic resonance relaxation in macromolecules. 2. Analysis of experimental results. *J. Am. Chem. Soc. 104*, 4559−4570.
(67) Scharadin, T. M., Adhikary, G., Shaw, K., Grun, D. J. B., Xu, W., and Eckert, R. L. (2014) Pericentrosomal localization of the TIG3 tumor suppressor requires an N-terminal hydrophilic region motif. *J. Invest. Dermatol. 134*, 1220−1229.
(68) Golczak, M., Sears, A. E., Kiser, P. D., and Palczewski, K. (2015) LRAT-specific domain facilitates Vitamin A metabolism by domain swapping in HRASLS3. *Nat. Chem. Biol. 11*, 26−32.
(69) Palmer, A. (2013) Protein dynamics from NMR spectroscopy and MD simulation. *Biophys. J. 104*, 45a.
(70) Krepl, M., Cléry, A., Blatter, M., Allain, F. H. T., and Sponer, J. (2016) Synergy between NMR measurements and MD simulations of protein/RNA complexes: application to the RRMs, the most common RNA recognition motifs. *Nucleic Acids Res. 44*, 6452−6470.
(71) Trbovic, N., Kim, B., Friesner, R. A., and Palmer, A. G., 3rd (2008) Structural analysis of protein dynamics by MD simulations and NMR spin-relaxation. *Proteins: Struct., Funct., Genet. 71*, 684−694.
(72) Zhang, L., Bouguet-Bonnet, S., and Buck, M. (2012) Combining NMR and molecular dynamics studies for insights into the allostery of small GTPase-protein interactions. *Methods Mol. Biol. 796*, 235−259.

https://doi.org/10.1021/acs.biochem.0c00974
Biochemistry 2021, 60, 1178−1190